A mangrove recognition index for remote sensing of mangrove forest from space

Xuehong Zhang[1,2,3,*] and Qingjiu Tian[3]

[1]Key Laboratory of Meteorological Disaster of Ministry of Education, and [2]School of Remote Sensing, Nanjing University of Information Science and Technology, Nanjing 210044, China
[3]International Institute for Earth System Science, Nanjing University, Nanjing 210093, China

Mangrove ecosystems, widely distributed in tropical and subtropical regions, can provide various ecological and economical ecosystem services. At the same time, mangrove forest belongs to the most threatened and vulnerable ecosystems worldwide and sustained a dramatic decline during the last half century. In this communication, a mangrove recognition index (MRI) has been developed for a quick monitoring of the extent and distribution of mangrove forest using remote sensing techniques. MRI is defined as $|GVI_L - GVI_H| * GVI_L * (WI_L + WI_H)$, where GVI and WI represent greenness vegetation index and wetness index respectively, obtained by Tasseled cap transformation. The former expresses the vegetation characteristics and the latter conveys the water information. The subscripts L and H denote low-tide level and high-tide level respectively. As a result, due to the unique nearshore wetland habitat of mangrove forest, MRI can respond sensitively its spectral signals and bigger the MRI of a pixel more likely that it belongs to mangrove forest. While MRIs of other ground covers, such as terrestrial vegetation, water, bare soil, etc. are less than that of mangrove forest. Combining multitemporal Landsat TM images with different tide levels, the mangrove forest in Beilunhekou National Nature Reserve Area of China is used to demonstrate the usefulness of MRI.

Keywords: Mangrove forest index, remote sensing, Tasseled cap transformation, tide level.

MANGROVE forest index is the dominant wetland in the intertidal ecosystems found along tropical and subtropical intertidal coastlines, that links terrestrial and marine systems[1]. It also provides various ecological and economical ecosystem services, including shoreline stabilization, reduction of coastal erosion, sediment and nutrient retention, storm protection, flood and flow control and water filtration[2,3]. However, mangrove forest belongs to the most threatened and vulnerable ecosystems worldwide[2–4]. The habitat area loss during the last two decades is estimated to be about 36% of the total global mangrove area[5].

Remote sensing has been widely proven to be essential in monitoring and mapping highly threatened mangrove ecosystems[6–8]. The monitoring and mapping of mangrove forest at a large scale mainly involves the use of medium-resolution multispectral imagery, such as Landsat Multispectral Scanner (MSS)[7,9–12], Landsat Thematic Mapper (TM) or Enhanced Thematic Mapper Plus (ETM$^+$)[7,13–15], SPOT[11,15–17] and Advanced Spaceborne Thermal Emission and Reflect Radiometer (ASTER)[18–20]. The methods used for the identification or extraction of mangrove forest mainly include visual interpretation[11,21], supervised classification[7,8,13,15,22], unsupervised classification[10,14,22,23], neural network classification[12,24], object-based method[9,25,26], etc. The imagery features extracted from remotely sensed imagery for mangrove forest identification are mostly the reflective spectral characteristics, vegetation indices or ratio indices, such as Normalized Difference Vegetation Index (NDVI)[27–30], TM3/TM5 (ref. 27), TM5/TM4 (ref. 27), modified normalized difference water index (MNDWI)[29,30] and normalized difference pond index (NDPI)[29,30].

Until recently, remotely sensed imagery at single tide was usually used in order to obtain the extent, and spatial distribution pattern of mangrove forest in a certain area and at a specified time using remote sensing techniques. However, the spectral signature of mangrove forest usually differs with the tide level change due to the intertidal effects (Figure 1). This also implies that the mapping

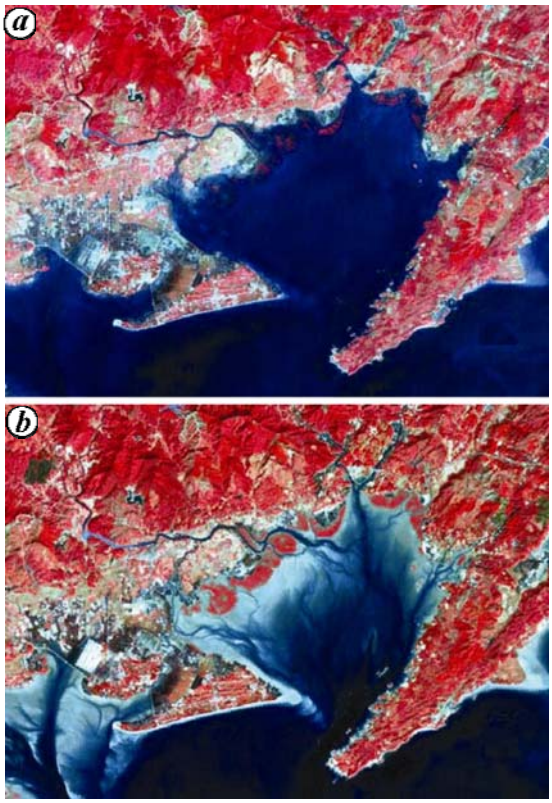

Figure 1. False colour composites of TM image at (***a***) high tide (30 October 2006) and (***b***) low tide (17 December 2006) with a band combination of 4-3-2 (R-G-B). The mangrove is beyond coastline and has a red image response. The terrestrial vegetation is within coastline and also has a red image response, wet soil has a grey colour, and soil or artificial facilities have a white or whitish-grey tone. Water has variable blue colours.

*For correspondence. (e-mail: zxhbnu@gmail.com)

accuracy of mangrove forest evidently depends on the tide level when using single-tide remote sensing imagery. On the contrary, if we make good use of the coastal wetland habitat of mangrove forest, i.e. the wetland background and periodical variation of the tide level, the remote sensing identification accuracy of mangrove forest will be improved. The objective of this study was to propose a spectral index – mangrove recognition index (MRI), which will be able to completely describe the unique characteristics of mangrove forest, i.e. near-shore coastal wetland habitat, for remote sensing of mangrove forest from space and to accurately map the status and distribution of mangrove forest.

MRI is defined as

$$\mathrm{MRI} = |\mathrm{GVI_L} - \mathrm{GVI_H}|*\mathrm{GVI_L}*(\mathrm{WI_L} + \mathrm{WI_H}), \quad (1)$$

where GVI and WI represent greenness vegetation index and wetness index respectively, obtained by Tasseled cap transformation[31]. This is an orthogonal transformation of the original remotely sensed data space to a new feature space. It can provide brightness index (BI), GVI and WI for Landsat TM data.

$$\mathrm{BI} = 0.0243_{\mathrm{tm1}} + 0.4158_{\mathrm{tm2}} + 0.5524_{\mathrm{tm3}} + 0.5741_{\mathrm{tm4}} + 0.3124_{\mathrm{tm5}} + 0.2303_{\mathrm{tm7}}, \quad (2)$$

$$\mathrm{GVI} = -0.1603_{\mathrm{tm1}} - 0.2819\mathrm{t}_{\mathrm{m2}} - 0.4939_{\mathrm{tm3}} + 0.794_{\mathrm{tm4}} - 0.0002_{\mathrm{tm5}} - 0.1446_{\mathrm{tm7}}, \quad (3)$$

$$\mathrm{WI} = 0.0315_{\mathrm{tm1}} + 0.2021_{\mathrm{tm2}} + 0.3102_{\mathrm{tm3}} + 0.1594_{\mathrm{tm4}} - 0.6806_{\mathrm{tm5}} - 0.6109_{\mathrm{tm7}}. \quad (4)$$

The subscript L and H denote low-tide level and high-tide level respectively. GVI describes the vegetation characteristics and WI provides the water information. The low-tide level and high-tide level can represent the tidal condition change of marine environment. $|\mathrm{GVI_L} - \mathrm{GVI_H}|$ can describe the GVI change of vegetation between the low-tide level and the high-tide level. Because the time is short, e.g. several hours, one day or several days, the $|\mathrm{GVI_L} - \mathrm{GVI_H}|$ is usually very small for other ground covers, including terrestrial vegetation, inland wetland vegetation and non-vegetation, whereas it is large for coastal vegetation, e.g. mangrove forest due to the tidal inundation. $\mathrm{GVI_L}$ can effectively reflect vegetation information, including mangrove forest, while $\mathrm{GVI_H}$ will omit most of the mangrove forest in lower and moderate intertidal zones, especially 'pioneering mangrove' due to the low terrain, low density and/or small stature. In addition, the values of $|\mathrm{GVI_L} - \mathrm{GVI_H}|$ and $\mathrm{GVI_L}$ for coastal sea grasses, due to their shallow water habitats, are usually far less than that of mangrove forest. $\mathrm{WI_L} + \mathrm{WI_H}$ is very big for mangrove forest and this can improve the separability between mangrove forest and other terrestrial ground covers, especially for terrestrial vegetation which is often mistakenly discriminated from mangrove forest. Therefore, bigger the MRI of a pixel, more likely that it belongs to mangrove forest. MRIs of other ground covers, such as terrestrial vegetation, water, inland wetland vegetation, bare soil, building, etc. are less than that of mangrove forest. Consequently, MRI has the ability to fully depict the properties of near-shore coastal wetland habitat, including the periodical variation of tide level and can be used to effectively recognize mangrove forest from remotely sensed imagery.

In order to show that MRI can be used for remote sensing mangrove forest from space, combining multi-temporal Landsat TM images with different tide levels, the mangrove forest in Beilunhekou National Nature Reserve Area, Fangchenggang City, Guangxi Zhuang Autonomous Region of China, located at 21°28′–21°37′N, 108°2′–108°16′E has been used. The study area locates in Beilunhekou National Nature Reserve Area. It is a nature reserve area protecting the mangrove ecosystems. The coastline belongs to the southern subtropical zone maritime monsoon climate. The main mangrove communities are *Avicennia marina*, *Aegiceras corniculatum*, *Kandelia candel*, *Bruguiera gymnorrhiza* and *Acanthus ilicifolius*, etc. The tidal type of the study area is regular diurnal, and the mean and maximum tidal range are 2.24 and 5.64 m respectively[32].

The *in situ* field survey was carried out at 15 mangrove forest sites, 20 terrestrial vegetation sites, 12 tidal flat sites, 10 bare soil sites and seven artificial facilities sites during 1–5 November 2006. The area of each field site is about 100 m × 100 m. During the field campaign, the location of each field site was determined using Differential Global Position System (DGPS) with a probable circle error of 2–5 m, which helped recognize training areas and assess the mapping accuracy of mangrove forest at the studied site. To assess the mapping accuracy of mangrove forest, training samples and validating samples were directly collected from these cloud-free TM images by combining the field survey data with visual interpretation due to the very distinctive difference between mangrove forest and other objects. The ground covers were categorized into mangrove forest and non-mangrove forest (including terrestrial vegetation, tidal flat, bare soil, artificial facilities and water). The training pixels numbers of each ground cover were 687 and 2824 respectively. The validating pixels numbers were 497 and 2168 respectively. Terrestrial vegetation consisted of crops that included cassava (*Manihot esculenta*), sugarcane (*Saccharum*) and woody plants. The woody species mainly included masson pine (*Pinus massoniana* L.), acacia (*Acacia confusa*) and Eucalyptus (mainly *Eucalyptus grandis* × *Eucalyptus urophylla*). Artificial facilities included buildings and roads.

Multi-tide remotely sensed images were derived from Landsat 5 TM. It is difficult to continuously acquire the

cloud-free optical images due to the restriction of climate at the study area. Consequently, two Landsat 5 TM images (path 125, row 45) dated 30 October 2006 (Figure 1 *a*) and 17 December 2006 (Figure 1 *b*) were obtained, whose tide levels at the time of image acquisition were 417 and 124 cm respectively. The tidal height datum plane was 230 cm below mean sea level[33]. Images selected were unaffected by atmospheric dust and were cloud-free. The image processing included image pre-processing and Tasseled cap transformation. The ENVI version 4.3 digital image processing software (ITT Industries Inc., USA) was used. The image pre-processing involved two main steps – image corrections (including radiometrical and geometrical correction) and image subsets. The two raw images used in the study were first converted to radiance images by means of the calibration coefficients of Landsat TM[34], and the radiance then converted to top-of-atmosphere (TOA) reflectance by normalizing for solar elevation and solar spectral irradiance[35]. Finally atmospheric correction was performed using the improved dark object subtraction technique[36,37] to derive surface reflectance from apparent reflectance. Geometric corrections were then performed on the two images. The image of high-tide level (dated 30 October 2006) was first geometrically registered to a Universal Transverse Mercator (UTM) projection and World Geodetic System-84 (WGS-84) datum, using a 1 : 50,000 topographic map and an image to map correction with 11 ground control points. The image of low-tide level (dated 17 December 2006) was then registered to the image of high tide level. After the image corrections, the subset images were extracted from the satellite scene. The Tasseled cap transformation was used on Landsat TM remote sensing images both high-tide level and low-tide level, and WI and GVI at different tide levels were extracted.

Because the terrain determines the scope of the intertidal effects on the spectral signal of mangrove forest, the latter is further divided into the mangrove forest in moderate/lower intertidal zone and mangrove forest in upper intertidal zone, denoted here as 'low mangrove' and 'high mangrove' respectively. In addition, the spectra of low mangrove at high tide are similar to mixed pixel of inland water and terrestrial vegetation, denoted as 'Aqu-veg'. Consequently, the spectral characteristics of Aqu-veg are also considered here. In order to understand the spectral characteristics of typical vegetation at the study area, training pixels of the low mangrove, high mangrove, terrestrial forest, Aqu-veg, crops, bare soil (cropland became bare soil at low-tide level) were randomly collected from the cloud-free subset images by combining the field survey and visual interpretation method, which were 488, 130, 524, 170, 144 and 327 points respectively. Figure 2 *a* and *b* illustrates reflectance spectra of typical vegetation, i.e. terrestrial forest, mangrove forest, and crops in low-tide level and high-tide level in the study area respectively.

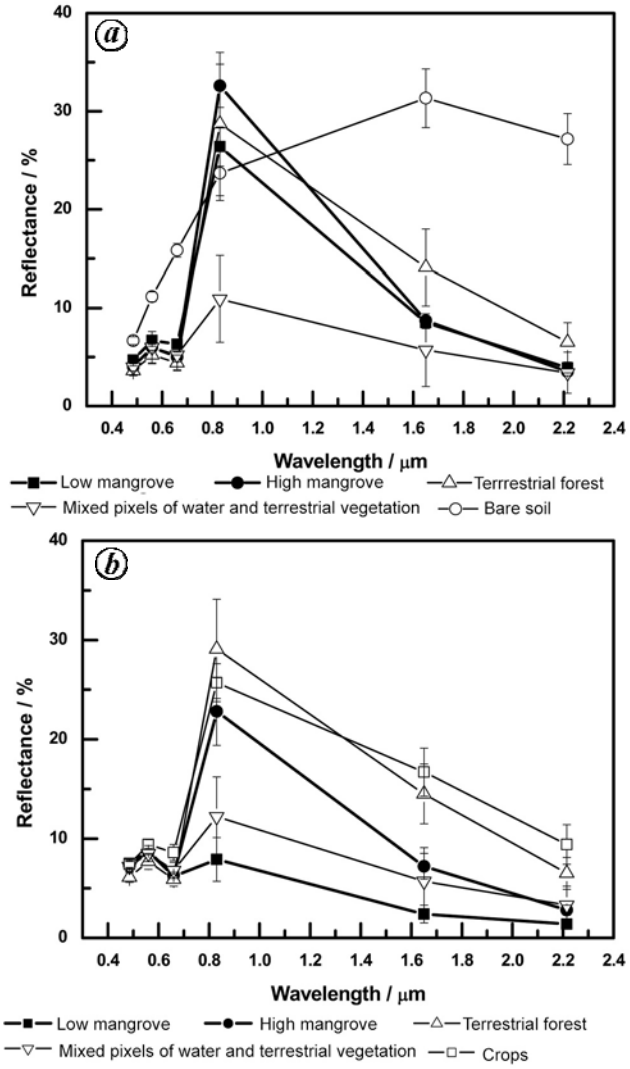

Figure 2. Spectral reflectance curves of typical vegetation, i.e. low mangrove, high mangrove, Aqu-veg (denotes mixed pixels of inland water and terrestrial vegetation), terrestrial forest and crop at (***a***) low tide and (***b***) high tide in the study area.

At low tide, spectra of both low mangrove and high mangrove are extremely similar to terrestrial forest, and there is obvious spectral overlapping between them. All the spectra of mangrove forest resemble those of Aqu-veg, except near the infrared region. The cropland became bare soil because the crops were reaped on 17 December 2006. Consequently, the spectrum appears to resemble that of bare soil and is evidently different from mangrove forest.

At high tide, extensive mangrove forest was inundated due to the rise of tide level, especially for the low mangrove. Hence, comparing with the low-tide level, the reflectance of mangrove forest sharply declines at high tide. The reflectance of low mangrove is smaller than that of Aqu-veg at both near-infrared region and shortwave-infrared region, and the spectral overlap zones evidently exist at all bands. The reflectance of high mangrove

markedly decreases at near-infrared region with the increase in the tide level. But the reflectance of high mangrove is similar to the terrestrial forest, except shortwave-infrared region. At the time of the high-tide level, i.e. on 30 October 2006, crops were not reaped, but they were becoming mature. Therefore, the reflectance values of crops apparently are very high at visible bands, and the spectra curve of high mangrove is slightly different from crops both at shortwave infrared bands and visible bands (especially at red band).

After the comparison of the spectra between mangrove forest and other vegetation types at different tide levels, it can be found that the reflectance spectra of mangrove forest are determined by the terrain they are located in as well as tide level. Consequently, in order to accurately discriminate mangrove forest from other vegetation types, we can employ the multi-temporal remotely sensed imagery with different tide levels and make good use of the coastal wetland background of mangrove forest and its spectral change with the tide level.

The identification accuracy of mangrove forest by remote sensing method is chiefly dominated by the separability between mangrove forest and other vegetation types. Therefore, spectral characteristics or indices for identifying mangrove forest from other vegetation types are compared below. *M*-statistic is employed to assess goodness of these spectral characteristics or indices[38]. The *M*-statistic tests the separation between the histograms produced by plotting the frequency of all the pixel values within two classes, and is defined as follows

$$M = \frac{|\mu_1 - \mu_2|}{\sigma_1 + \sigma_2}, \tag{5}$$

where M is the normalized mean distance and μ_1, μ_2 are mean values for class 1, class 2. σ_1, σ_2 are standard deviations for class 1, class 2. $M < 1$ indicates that the classes significantly overlap and the ability to separate (or discriminate) classes is poor, while $M > 1$ means good class separation; and bigger the M value better is the separability between the classes.

In Table 1, TM_i (the origin reflectance of each band of Landsat TM), BI, WI, GVI, NDVI, MRI, $NDVI_L - NDVI_H$ (the subscript L and H denoted low-tide level and high-tide level respectively), $WI_L + WI_H$, $GVI_L - GVI_H$, $BI_L - BI_H$, MNDWI (MNDWI = (Green – MIR)/(Green + MIR))[29,30] has been extracted from Landsat TM remote sensing images of high-tide level and low-tide level. The *M*-statistic values between mangrove and other vegetation types were further calculated by the training samples of each class (in Table 1).

For terrestrial forest, the *M*-statistic values are all very small when using the original reflectance spectra at low tide. The *M*-statistic value of $TM3_L$ between low mangrove and terrestrial forest is maximal, but it is only 1.52. If the reflectance spectra at high tide are employed, the separability between mangrove forest and terrestrial forest can be improved. For example, when using $TM5_H$, the *M*-statistic value increases to 3.13 and 1.72 for low mangrove and high mangrove respectively. The features extracted by Tasseled cap transformation can clearly improve the separation ability between mangrove forest and terrestrial forest. Typically for high mangrove, the *M*-statistic values increase to 2.35 and 2.22 at both low tide and high tide respectively when using WI. The separability can be further improved by adopting the tide information about mangrove forest. Especially for high mangrove, its *M*-statistic value increases to 2.54 by combining images at low tide and high tide, i.e. $WI_L + WI_H$.

Among the *M*-statistic values between mangrove forest and Aqu-veg, only the *M*-statistic values of $TM4_L$ are large by adopting the original reflectance spectra at low tide, and they are 2.40 and 3.26 for low mangrove and high mangrove respectively. GVI can slightly increase the *M*-statistic values between mangrove forest and Aqu-veg, which are 2.47 and 3.60 for low mangrove and high mangrove respectively. Further combining low tide image and high tide image, the features of $BI_L - BI_H$ and $GVI_L - GVI_H$ can improve the *M*-statistic values between low mangrove and Aqu-veg, and they are 2.88 and 3.08 respectively.

The cropland became bare soil because the crops were reaped at the time of low tide image acquisition. They were not reaped at the time of high tide image acquisition, as the crops were in the maturing period. Therefore, their reflectance spectral characteristics are similar to and meantime slightly different from the terrestrial forest (Figure 2 *b*). The *M*-statistic values between mangrove forest and crops are also similar to those of terrestrial forest, except TM1 and TM3. In addition, crops were not reaped at the time of the high-tide level, as they were maturing. This caused the reflectance values to increase compared to those before maturation at visible region, especially for TM3. Therefore, the *M*-statistic values between high mangrove and crops are quite different for both TM3 and TM4 (2.08 and 0.54 respectively).

MRI can fully depict the properties of near-shore coastal wetland habitat and the periodical variation of tide level. Consequently, it can effectively recognize mangrove forest from other vegetation classes (Table 1). In addition, the classification features for mangrove forest identification are usually extracted from single-tide remote sensing images and the original reflective spectral features, vegetation indices or ratio indices, such as NDVI, TM3/TM5, TM5/TM4, MNDWI are chiefly employed. Among the above indices, at both low tide and high tide, only TM3/TM5 and MNDWI can effectively discriminate mangrove forest (both low mangrove and high mangrove) from terrestrial forest as well as crops, and TM5/TM4 only slightly differentiates high mangrove from terrestrial forest as well as crops. Nevertheless, it is

Table 1. The *M*-statistic values between mangrove forest and other vegetation types

Classification features	Low mangrove			High mangrove		
	Terrestrial forest	Aqu-veg[2]	Crops	Terrestrial forest	Aqu-veg	Crops
$TM1_L$[1]	1.27	0.51	/[3]	0.42	0.07	/
$TM2_L$	1.17	0.37	/	0.68	0.02	/
$TM3_L$	1.52	0.59	/	0.43	0.11	/
$TM4_L$	0.25	2.40	/	0.40	3.26	/
$TM5_L$	1.28	0.65	/	1.28	0.72	/
$TM7_L$	1.06	0.17	/	1.23	0.02	/
$TM1_H$[1]	1.56	0.35	0.21	1.35	0.12	0.06
$TM2_H$	0.94	0.21	0.95	0.94	0.21	0.94
$TM3_H$	0.42	0.59	2.26	0.50	0.47	2.08
$TM4_H$	2.93	0.70	4.34	0.75	1.44	0.54
$TM5_H$	3.13	0.77	4.33	1.72	0.32	2.58
$TM7_H$	2.46	0.83	3.30	1.71	0.2	2.65
BI_L[4]	0.39	1.51	/	0.16	1.71	/
GVI_L[4]	0.41	2.47	/	0.35	3.60	/
WI_L[4]	2.00	0.92	/	2.35	1.25	/
BI_H	2.97	0.74	4.83	1.07	0.80	2.05
GVI_H	2.96	0.69	3.83	0.81	1.52	0.24
WI_H	2.47	0.75	3.03	2.22	0.63	2.77
$WI_L + WI_H$	2.38	0.94	/	2.54	1.07	/
$GVI_L - GVI_H$	2.76	3.08	/	1.83	2.12	/
$BI_L - BI_H$	3.06	2.88	/	1.18	1.17	/
$NDVI_L$	1.02	1.59	/	0.10	2.38	/
$NDVI_H$	3.04	0.67	2.38	0.80	1.66	0.57
$TM5_L/TM4_L$	1.22	0.82	/	1.81	1.16	/
$TM5_H/TM4_H$	1.45	0.66	2.38	1.58	0.67	2.64
$TM3_L/TM5_L$	3.28	0.63	/	1.92	0.86	/
$TM3_H/TM5_H$	2.57	0.75	2.51	1.87	0.70	1.61
$MNDWI_L$[4]	2.16	1.10	/	2.68	1.01	/
$MNDWI_H$	3.63	0.38	3.07	2.37	0.58	2.64
MRI	2.93	3.85	/	2.77	3.75	/

[1]The subscripts L and H denote low tide level and high tide level respectively. TM_i denotes the reflectance of band *i* of Landsat TM.
[2]Aqu-veg denotes mixed pixels of inland water and terrestrial vegetation.
[3]The cropland became bare soil at the time of image acquisition at low tide, i.e. 17 December 2006.
[4]MNDWI is defined as $(TM_2 - TM_5)/(TM_2 + TM_5)$ in this communication.

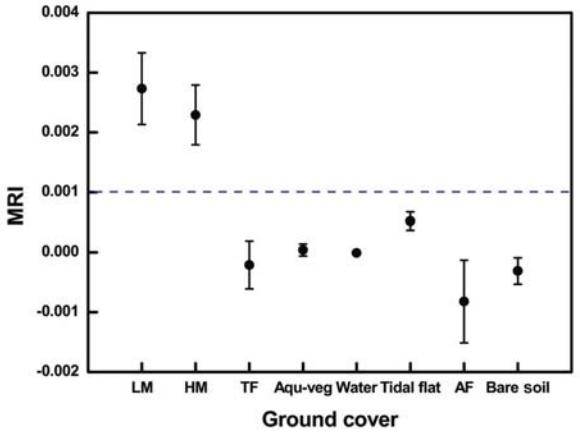

Figure 3. The plotted mean values of mangrove recognition index (MRI) showing the difference between mangrove forest and non-mangrove forest. Bars show the standard deviation. LM, HM, TF, Aqu-veg and AF are the abbreviations for low mangrove, high mangrove, terrestrial forest, mixed pixels of inland water and terrestrial vegetation and artificial facilities respectively.

difficult to distinguish mangrove forest from Aqu-veg. NDVI can only slightly differentiate high mangrove from Aqu-veg at both low tide and high tide, but cannot identify high mangrove from terrestrial forest as well as crops. For low mangrove, NDVI can only slightly distinguish it from Aqu-veg at low tide and from terrestrial forest as well as crops at high tide.

Based on the above analysis, for the image both at low tide and high tide, a single image does not effectively discriminate mangrove forest from other vegetation types. When considering the unique near-shore wetland habitat of mangrove forest, the ability to separate mangrove from other vegetation types as well as Aqu-veg can be enhanced.

Figure 3 shows the MRI of low mangrove, high mangrove, terrestrial forest, Aqu-veg, tidal flat, water, artificial facilities and bare soil. The MRI value of crops is not considered in Figure 3 because the cropland became bare soil at the time of image acquisition at low tide. But the MRI value should be similar to that of terrestrial forest because of the spectral similarity between them (see Figure 2 *b*). Due to the intertidal effects, the MRI values of mangrove forest are obviously greater than non-mangrove forest. The former is greater than 0.001 and the latter is less than 0.001. Consequently, MRI is good for discrimi-

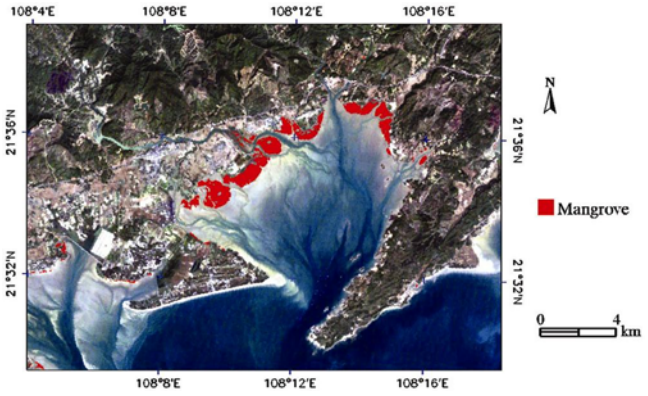

Figure 4. The mangrove distribution map responding the red image tone, produced from MRI for Beilunhekou National Nature Reserve Area, Fangchenggang City, Guangxi Zhuang Autonomous Region, China. The background image is the natural colour composite of low-tide level TM image.

nating mangrove forest from non-mangrove forest. Based on the above analysis, 0.001 is selected as the threshold value of MRI based on Figure 3 in order to extract mangrove forest. Figure 4 depicts the spatial distribution of mangrove forest responding the red image tone, in the study area by overlaying the natural colour composite TM image at low tide and produced from MRI. The accuracy assessment of mangrove forest was obtained by comparing the classified data with the validating data. The classification accuracies of mangrove forest are as follows: producer's and user's accuracies are 93.19% and 98.09% respectively.

In conclusion, MRI is proposed for remote sensing of mangrove forest from space using multi-temporal Landsat TM images with different tide levels in Beilunhekou National Nature Reserve Area of China. This index considers the intertidal effects and is sensitive to the wetness, greenness and change of greenness. MRI of mangrove forest is much greater than that of non-mangrove forest due to the coastal habitat of the former. Limited test of this index using TM data demonstrated that MRI can effectively extract mangrove forest. However, the superiority of MRI is limited to some factors as follows: (a) The band span of the remote sensor adopted. The index involves visible bands, near-infrared bands and short-wave-infrared bands; otherwise MRI will not be established. (b) The amount of selected tidal range. MRI uses intertidal effects to extract mangrove forest and larger the tidal range, better is the separability between mangrove forest and other ground covers. Therefore, the selected tidal range should be as large as possible, such as high water spring tide and high water neap tide. (c) The time between low tide and high tide. If it is too long, not only mangrove forest, but the non-mangrove forest will sharply change. This is bound to affect the ability of MRI to extract mangrove forest.

1. Rasolofoharinoro, M., Blasco, F., Bellan, M. F., Aizpuru, M., Gauquelin, T. and Denis, J., A remote sensing based methodology for mangrove studies in Madagascar. *Int. J. Remote Sensing*, 1998, **19**, 1873–1886.
2. Alongi, D. M., Mangrove forests: resilience, protection from tsunamis, and responses to global climate change. *Estuarine, Coastal Shelf Sci.*, 2008, **76**, 1–13.
3. Blasco, F., Saemger, P., and Janodet, E., Mangroves as indicators of coastal change. *Catena*, 1996, **27**, 167–178.
4. Ellison, J., Mangrove retreat with rising sea level, Bermuda. *Estuarine, Coastal Shelf Sci.*, 1993, **37**, 75–87.
5. FAO, The world's mangroves 1980–2005. FAO Forestry Paper 153, FAO: Rome, Italy, 2007; ftp://ftp.fao.org/docrep/fao/010/a1427e/a1427e00.pdf (accessed on 6 January 2013).
6. Green, E. P., Mumby, P. J., Edwards, A. J., Clark, C. D. and Ellis, A. C., The assessment of mangrove areas using high resolution multispectral airborne imagery. *J. Coastal Res.*, 1998, **14**, 433–443.
7. Howari, F. M., Jordan, B. R., Bouhouche, N. and Wyllie-Echeverria, S., Field and remote-sensing assessment of mangrove forests and seagrass beds in the northwestern part of the United Arab Emirates. *J. Coastal Res.*, 2009, **25**, 48–56.
8. Everitt, J. H., Yang, C., Judd, F. W. and Summy, K. R., Use of archive aerial photography for monitoring black mangrove populations. *J. Coastal Res.*, 2010, **26**, 649–653.
9. Berlanga-Robles, C. A. and Ruiz-Luna, A., Land use mapping and change detection in the coastal zone of northwest Mexico using remote sensing techniques. *J. Coastal Res.*, 2002, **18**, 514–522.
10. Giri, C., Zhu, Z., Tieszen, L. L., Singh, A., Gillette, S. and Kelmelis, J. A., Mangrove forest distributions and dynamics (1975–2005) of the tsunami-affected region of Asia. *J. Biogeogr.*, 2008, **35**, 519–528.
11. Prasad, P. R., Reddy, C. S., Rajan, K. S., Raza, S. H. and Dutt, C. B., Assessment of tsunami and anthropogenic impacts on the forest of the North Andaman Islands, India. *Int. J. Remote Sensing*, 2009, **30**, 1235–1249.
12. Seto, K. C. and Fragkias, M., Mangrove conversion and aquaculture development in Vietnam: a remote sensing-based approach for evaluating the Ramsar Convention on Wetlands. *Global Environ. Change*, 2007, **17**, 486–500.
13. Andriamparany, R. and Francois, F., Dynamics of mangrove forests in the Mangoky River Delta, Madagascar, under the influence of natural and human factors. *For. Ecol. Manage.*, 2010, **259**, 1161–1169.
14. Ferreira, M. A., Andrade, F., Banderiba, S. O., Cardoso, P., Nogueira Mendes, R. and Paula, J., Analysis of cover change (1995–2005) of Tanzania/Mozambique transboundary mangroves using Landsat imagery. *Aquat. Conserv.*, 2009, **19**, 38–45.
15. Lee, T. and Yeh, H., Applying remote sensing techniques to monitor shifting wetland vegetation: a case study of Danshui River estuary mangrove communities, Taiwan. *Ecol. Eng.*, 2009, **35**, 487–496.
16. Gao, J., A comparative study on spatial and spectral resolutions of satellite data in mapping mangrove forests. *Int. J. Remote Sensing*, 1999, **20**, 2823–2833.
17. Thu, P. M. and Populus, J., Status and changes of mangrove forest in Mekong Delta: case study in Tra Vinh, Vietnam. *Estuarine, Coastal Shelf Sci.*, 2007, **71**, 98–109.
18. Giri, C. and Muhlhausen, J., Mangrove forest distribution and dynamics in Madagascar (1975–2005). *Sensors*, 2008, **8**, 2104–2117.
19. Saito, H., Bellan, M. F., Al-Habshi, A., Aizpuru, M. and Blasco, F., Mangrove research and coastal ecosystem studies with SPOT-4 HRVIR and TERRA ASTER in the Arabian Gulf. *Int. J. Remote Sensing*, 2003, **24**, 4073–4092.
20. Vaiphasa, C., Andrew, S. K. and Willem, F. B., A post-classifier for mangrove mapping using ecological data. *ISPRS J. Photogr. Remote Sensing*, 2006, **61**, 1–10.
21. Selvam, V., Ravichandran, K. K., Gnanappazham, L. and Navamuniyammal, M., Assessment of community based restoration of

Pichavaram mangrove wetland using remote sensing data. *Curr. Sci.*, 2003, **85**, 794–798.
22. Paling, E. I., Kobryn, H. T. and Humphreys, G., Assessing the extent of mangrove change caused by cyclone Vance in the eastern Exmouth Gulf, northwestern Australia. *Estuarine, Coastal Shelf Sci.*, 2008, **77**, 603–613.
23. Giri, C., Pengra, B., Zhu, Z., Singh, A. and Tieszen, L., Monitoring mangrove forest dynamics of the Sundarbans in Bangladesh and India using multi-temporal satellite data from 1973 to 2000. *Estuarine, Coastal Shelf Sci.*, 2007, **73**, 91–100.
24. Mas, J. F., Mapping land use/cover in a tropical coastal area using satellite sensor data, GIS and artificial neural networks. *Estuarine, Coastal Shelf Sci.*, 2004, **59**, 219–230.
25. Myint, S. W., Giri, C. P., Wang, L., Zhu, Z. and Gillette, S. C., Identifying mangrove species and their surrounding land use and land cover classes using an object-oriented approach with a lacunarity spatial measure. *GISci. Remote Sensing*, 2008, **45**, 188–208.
26. Wang, L., Sousa, W. and Gong, P., Integration of object-based and pixel-based classification for mangrove mapping with IKONOS imagery. *Int. J. Remote Sensing*, 2004, **25**, 5655–5668.
27. Green, E. P., Clear, C. D., Mumby, P. J., Edwards, A. J. and Ellis, A. C., Remote sensing techniques for mangrove mapping. *Int. J. Remote Sensing*, 1998, **19**, 935–956.
28. Jensen, J. R., Lin, H., Yang, X., Ramset, E., Davis, B. A. and Thoemke, C. W., The measurement of mangrove characteristics in south-west Florida using SPOT multispectral data. *Geocartogr. Int.*, 1991, **2**, 13–21.
29. National Wetland Atlas, SAC/EPSA/ABHG/NWIA/ATLAS/34/2011, Space Applications Centre (ISRO), Ahmedabad, India, 2011; http://moef.nic.in/downloads/public-information/NWIA_Assam_Atlas.pdf (accessed on 6 January 2013).
30. Sushma Panigrahy, Murthy, T. V. R., Patel, J. G. and Singh, T. S., Wetlands of India: inventory and assessment at 1 : 50,000 scale using geospatial techniques. *Curr. Sci.*, 2012, **102**, 852–856.
31. Crist, E. P. and Cicone, R. C., Application of the tasseled cap concept to simulated Thematic Mapper data. *Photogramm. Eng. Remote Sensing*, 1984, **50**, 343–352.
32. Liang, S., Liu, J. and Liang, M., Ecological study on the mangrove communities in Beilunhekou National Nature Reserve. *J. Guangxi Normal University*, 2004, **22**, 70–76.
33. http://port.shippingchina.com/tide/index/ (accessed on 6 January 2013).
34. Chander, G. and Markham, B., Revised Landsat-5 TM radiometric calibration procedures and postcalibration dynamic ranges. *IEEE Trans. Geosci. Remote Sensing*, 2003, **41**, 2674–2677.
35. Thenkabail, P. S., Enclona, E. A., Ashton, M. S., Legg, C. and Dieu, M. J. D., Hyperion, IKONOS, ALI, and ETM+ sensors in the study of African rainforests. *Remote Sensing Environ.*, 2004, **90**, 23–43.
36. Chavez, P. S., An improved dark-object subtraction technique for atmospheric scattering correction of multispectral data. *Remote Sensing Environ.*, 1986, **24**, 459–479.
37. Chavez, P. S., Image-based atmospheric corrections – revisited and improved. *Photogramm. Eng. Remote Sensing*, 1996, **62**, 1025–1036.
38. Kaufman, Y. and Remer, L., Detection of forests using mid-IR reflectance: an application for aerosol studies. *IEEE Trans. Geosci. Remote*, 1994, **32**, 672–683.

ACKNOWLEDGEMENTS. This study was supported by the National Natural Science Foundation of China (Grant No. 41201461), the National Science and Technology Major Project (Grant No. 30-Y20A01-9003-12/13, China) and the project funded by the Priority Academic Programme Development of Jiangsu Higher Education Institutions.

Received 10 May 2013; accepted 17 May 2013

The Delhi 1960 earthquake: epicentre, depth and magnitude

S. K. Singh[1,*], G. Suresh[2], R. S. Dattatrayam[2], H. P. Shukla[2], S. Martin[3], J. Havskov[4], X. Pérez-Campos[1] and A. Iglesias[1]

[1]Instituto de Geofísica, Universidad Nacional Autónoma de México, Ciudad Universitaria, 04510 México, DF, México
[2]India Meteorological Department, Lodi Road, New Delhi 110 003, India
[3]Victoria University of Wellington, School of Geography, Environment and Earth Sciences, Wellington, New Zealand
[4]Department of Earth Sciences, University of Bergen, Bergen, Norway

Though the Delhi earthquake of 27 August 1960 is important in understanding seismic hazard to the city, there is large uncertainty associated with its reported epicentre, depth and magnitude. The reported epicentres given in different catalogues are not consistent with felt and damage reports, and the depths (58–109 km) are also inconsistent with recorded waveforms (including the excitation of *Lg* waves), decay of seismic intensities with distance, number of aftershocks, earthquake sound and seismotectonics of the region. The reported magnitude of the earthquake varies between 5.3 and 6.0. We have performed an exhaustive analysis of the available information, including comparison of the seismograms of the 1960 earthquake with six recent well-recorded events as well as with the Moradabad earthquake of 1966. We find that: (1) A more reliable epicentre as compared to the instrumentally determined one, is provided by the locus of the strongest seismic intensity: 28.47°N, 77.00°E (between Delhi Cantonment and Gurgaon). (2) The earthquake was shallow (depth ≤ 30 km, but most likely ≤ 15 km). (3) The magnitude of the earthquake was M_w 4.8 (range M_w 4.6–4.9). The seismic intensity is also consistent with $M_w < 5.0$. We conclude that the Delhi 1960 earthquake occurred between Delhi Cantonment and Gurgaon, it was shallow and its magnitude was 4.8, significantly less than *M* 6.0 often used in studies dealing with hazard in the city.

Keywords: Earthquake, epicentre, depth, magnitude, seismic hazard.

THE National Capital Territory (NCT) of Delhi, presently home to more than 16 million people, is vulnerable to earthquakes at local and regional distances as well as to great earthquakes along the Himalayan arc. Unfortunately, the information on historical seismicity in the NCT is plagued with large uncertainty. There appear to be two previous local earthquakes that were damaging. However, the location and magnitude of neither of these events are well constrained. The first one caused numerous fatalities

*For correspondence. (e-mail: krishnamex@yahoo.com)